Article

J. Biol. Regul. Homeost. Agents. 2023; 37(11): 6061–6072
https://doi.org/10.23812/j.biol.regul.homeost.agents.20233711.580

Protective Effect of Pharmacological SIRT2 Inhibition on Renal Dysfunction, Fibrosis, TGF-β1/β-Catenin, and Klotho Signaling in D-Galactose-Induced Aging Model

Arzu Keskin-Aktan[1,*], Aslı Nur Bahar[2], Fatma Gizem Sonugür[3], Saadet Özen Akarca-Dizakar[4], Kazime Gonca Akbulut[5]

[1]Department of Physiology, Faculty of Medicine, Afyonkarahisar Health Sciences University, 03200 Afyonkarahisar, Turkey
[2]Department of Physiology, Faculty of Medicine, Marmara University, 34722 İstanbul, Turkey
[3]Cancer Research Institute, Faculty of Medicine, Ankara University, 06760 Ankara, Turkey
[4]Department of Histology and Embryology, Faculty of Medicine, İzmir Bakırçay University, 35660 İzmir, Turkey
[5]Department of Physiology, Faculty of Medicine, Gazi University, 06790 Ankara, Turkey
*Correspondence: arzu.aktan@afsu.edu.tr; arzukeskinaktan@gmail.com (Arzu Keskin-Aktan)
Published: 20 November 2023

Background: Fibrosis induced by transforming growth factor-β1 (TGF-β1) activity and the Wnt/β-catenin pathway is a significant hallmark of progressive kidney disease and kidney aging. We aimed to investigate the effects of pharmacological silent mating type information regulation 2 homolog-2 (SIRT2) inhibition on renal functions, histopathological changes, fibrosis, TGF-β1/β-catenin and klotho signaling, and apoptosis in D-galactose (D-Gal)-induced aging model.

Methods: The study was conducted with three months old male rats divided into four groups: control (Saline solution (0.9%, 0.5 mL/day) was administered subcutaneously (sc) for ten weeks) (n = 6), D-Gal (D-galactose saline solution (150 mg/kg/day) was administered sc for ten weeks) (n = 8), D-Gal+DMSO (D-galactose (150 mg/kg/day) and 4% dimethyl sulfoxide (DMSO) in phosphate-buffered saline (PBS) (10 µL/bw/day) were administered sc for ten weeks) (n = 8), and D-Gal+acylglycerol kinase (AGK)-2 (D-galactose (150 mg/kg/day) and AGK-2 in 4% DMSO-PBS (10 µM/bw/day) was administered sc for ten weeks) (n = 8). The kidney index was calculated, renal function markers (sodium (Na^+), creatinine (Cr), blood urea nitrogen (BUN)) in plasma and urine samples were analyzed, and fractional excretion of sodium (FeNa%) was calculated. Glomerular diameter, fibrosis, and basement membrane thickness were analyzed with histopathological methods. TGF-β1 and β-catenin mRNA expression were determined with quantitative real-time polymerase chain reaction (qRT-PCR), klotho protein levels were determined with the enzyme linked immunosorbent assay (ELISA) method, and SIRT2 protein expression was determined with western blot. The immunohistochemical method was employed to determine the immunoreactivities of β-catenin, klotho, SIRT2, and fibronectin. Apoptosis was determined with the terminal deoxynucleotidyl transferase deoxyuridine triphosphate (dUTP) nick end labeling (TUNEL) method.

Results: AGK-2 and D-galactose co-administration increased kidney index and decreased plasma and urine Na^+ and Cr levels, as well as BUN and FeNa% ($p < 0.05$). AGK-2 improved the histopathological changes induced by D-galactose, reducing fibrosis and basal membrane thickness ($p < 0.05$). Furthermore, AGK-2 administration decreased TGF-β1, β-catenin, SIRT2, and fibronectin in the kidney ($p < 0.05$). AGK-2 and D-galactose co-administration increased klotho protein levels in the kidney; however, the increase was not statistically significant in klotho immunoreactivity ($p > 0.05$). D-galactose induced apoptosis in the kidney ($p < 0.05$); however, AGK-2 did not significantly mitigate apoptosis ($p > 0.05$).

Conclusion: Our findings suggested that pharmacological SIRT2 inhibition could ameliorate alterations in functional, histopathological, and fibrosis protein pathway activities in the kidney that are associated with aging.

Keywords: D-galactose; fibrosis; kidney; SIRT2 inhibition; TGF-β1

Introduction

Aging is among the most significant chronic kidney disease (CKD) risk factors. CKD is about three times more prevalent in individuals who are 65 or older when compared to those who are 45–64 years older and about five times more prevalent when compared to those who are 18–44 years old (33.7% vs. 12.3%, 6.3%) [1]. Furthermore, the World Health Organization established that kidney diseases were the tenth cause of disease mortality [2].

Micro-anatomical changes that are observed in the kidneys of the elderly include nephrosclerosis and nephron hypertrophy. Macro-anatomical changes entail reduced cortical volume and a high incidence of renal tumors, of-

Journal of
BIOLOGICAL REGULATORS
and Homeostatic Agents

ten benign. Furthermore, a decrease in functional mass correlates with a decline in kidney index in aging kidneys [3]. Changes in the permeability of glomerular capillary walls, podocyte damage, apoptosis, tubular functions, urine composition, hormones, and bioactive molecules associated with aging lead to a decrease in glomerular filtration rate (GFR). In the analysis of kidney functions and damages, serum and urine GFR, albumin, sodium (Na), potassium (K), chloride (Cl), and creatinine (Cr) levels, and blood urea nitrogen (BUN) and fractional excretion of sodium (FeNa%) are significant renal function markers [4–6].

Fibrosis is a prominent indicator of kidney disease development, especially in older renal systems. The transforming growth factor-β (TGF-β) signal induces fibrosis by promoting the differentiation of fibroblasts into myofibroblasts after injury. In the extracellular matrix (ECM), fibrous proteins such as structural proteins, collagens, adhesive proteins, and fibronectin are more prominent [7]. The TGF-β signal induces renal fibrosis not only through direct transcriptional changes but also by regulating the Wnt/β-catenin, klotho/FGF23, and YAP/TAZ signaling pathways [8,9].

Due to the ease of application, low cost, short duration, and high survival rate, accelerated rodent aging models are preferred over natural aging models. The D-galactose-induced accelerated aging model is still the most prevalent rodent model due to its minimal side effects during the experiments and higher survival rate [6,10]. Naturally present in the body, D-galactose is an aldohexose and a reducing sugar present in nutrients such as milk, milk products, and various fruits and vegetables. The potential mechanisms entailed in high-dose D-galactose-induced aging and age-related changes are as follows: (1) Mitochondrial dysfunction induced by galactose via reduction by galactose reductase, (2) disruption of redox homeostasis by galactose oxidase oxidation, and (3) the increase in advanced glycation end products (AGEs), AGE receptors, and nicotinamide adenine dinucleotide phosphate oxidase via non-enzymatic glycation. Oxidative stress, inflammation, and apoptosis induced by these three fundamental pathways lead to aging and degenerations associated with aging [10].

The aging model induced by chronic administration of high D-galactose dose is commonly employed in anti-aging studies conducted on the kidney. D-galactose administration to 1–3 months (6–20 weeks) old rodents mimics degenerative changes in the kidneys of naturally aged (~24 months) rodents. These changes entail oxidative stress markers (such as malondialdehyde, 8-OHdG formation, etc.), inflammation indicators (NF-κB, TNFα, IL-6, etc.), urinary blood markers (BUN, Cr, uric acid, cystatin C, etc.), and histological alterations (including the number and diameter of normal/sclerotic glomeruli, expansion of the renal capsule, basal membrane thickness, apoptosis/necrosis, etc.) [3,4,6,10].

D-galactose administration leads to an increase in renal TGF-β expression and a decrease in klotho [11]. The Wnt/β-catenin upregulation that induces renal fibrosis could be antagonized by klotho. Furthermore, klotho could also inhibit fibronectin and α-SMA [12]. The expression of the anti-aging gene klotho, primarily expressed in the distal tubular cells in the kidney, decreases with aging [13]. Klotho acts as a Wnt/β-catenin signal antagonist [14] and inhibits renal fibrosis by downregulating the TGF-β signal [15].

The sirtuins, known as longevity proteins (SIRT1-7), are the members of nicotinamide adenine dinucleotide (NAD)-dependent class III histone deacetylase family. Changes in the expression of the silent mating type information regulation 2 homolog-2 (SIRT2), primarily located in the cytoplasm, are associated with metabolic homeostasis, neurodegenerative diseases, tumor development, and inflammation [16]. Sirtuins play a significant role in myofibroblast differentiation, and it was demonstrated that SIRT2 has profibrotic effects on the kidney [17,18]. The correlation between SIRT2 and transforming growth factor-β1 (TGF-β1) in various tissues, including the kidneys [19], lungs [20], and liver [21] suggests that SIRT2 plays a key regulatory role in fibrosis in addition to fibrosis development.

A few *in vivo*/*in vitro* studies demonstrated the protective effect of pharmacological SIRT2 inhibition with the specific SIRT2 inhibitor acylglycerol kinase (AGK)-2 (2-Cyano-3-[5-(2,5-dichlorophenyl)-2-furanyl]-N-5-quinolinyl-2-propenamide) in kidneys [19,22]. It was reported that AGK-2 had antifibrotic effects in the liver [21] and lung [20,23]. In our previous studies, we demonstrated the protective effect of SIRT2 in the aging of the brain [24,25] and the liver [21]. Based on current knowledge, we hypothesized that SIRT2 inhibition could also ameliorate renal fibrosis that accompanies renal aging. There are no studies in the literature that demonstrated the protective effect of SIRT2 inhibition in kidneys in D-galactose-induced aging or natural aging. In our study, we aimed to investigate the effects of pharmacological SIRT2 inhibition via AGK-2 on renal functions, histological changes, TGF-β1/β-catenin and klotho-mediated fibrosis development, and apoptosis in D-galactose-induced renal aging model.

Methods

Animals

The study was conducted with 32 young (three-month-old) male Sprague Dawley rats, where two rats were designated for the preliminary study. The study was approved by the Gazi University Local Ethics Committee for Animal Experiments (G.U.ET-20.011). The animals were procured from Gazi University Laboratory Animals and Experimental Research Center and housed in standard laboratory conditions with a 12 h light/dark cycle (Light between 08.00

and 20.00 h) at 23 °C, and commercial rat chow and ad libitum tap water were fed to the rats. Thirty male rats (244.43 ± 11.89, g) were randomly divided into four groups, and there was no significant difference between the mean body weight of the groups. The D-galactose and AGK-2 doses were determined based on the previous studies in the literature and our preliminary study findings. A detailed discussion and preliminary study findings are presented in the **Supplementary Material**.

Treatment Groups

(1) Control Group (n = 6): Saline solution (0.9%, 0.5 mL/day) was administered subcutaneously (sc) for ten weeks.

(2) D-galactose (D-Gal) Group (n = 8): D-galactose saline solution (150 mg/kg/day) was administered sc for ten weeks.

(3) D-Gal+DMSO Group (n = 8): D-galactose (150 mg/kg/day) and 4% dimethyl sulfoxide (DMSO) in phosphate-buffered saline (PBS) (10 µL/bw/day) were administered sc for ten weeks.

(4) D-Gal+AGK2 Group (n = 8): D-galactose (150 mg/kg/day) and AGK-2 in 4% DMSO-PBS (10 µM/bw/day) was administered sc for ten weeks.

To collect blood from the heart, rats were anesthetized with ketamine (80 mg/kg, ip) / xylazine (10 mg/kg, ip). After their kidneys were removed and weighed, rats were sacrificed under deep anesthesia. The right kidney was used for mRNA and protein analysis, while the left kidney was utilized for histological examination.

Measurements of Kidney Index and Renal Function Markers

The kidney index was calculated by normalizing the total sum of the ratio of wet kidney weight to the body weight. The kidney index formula was as follows: "[total weight of right and left kidneys (mg) / body weight (g)] × 100". To analyze the kidney functions, plasma sodium (Na^+), creatinine (Cr), blood urea nitrogen (BUN), and urine Na^+ and Cr levels were measured with an automatic biochemical analyzer. Furthermore, the FeNa% excretion was calculated with the formula: "FeNa (%) = [(urinary Na × serum Cr) / (urinary Cr × serum Na)] × 100".

Histopathological Analysis

The left kidneys were fixed in 10% formaldehyde for histological and immuno-histological analysis and routine histological techniques were employed to prepare the samples for staining. The analysis of histopathological and histo-morphological changes in kidney tissues (glomerular diameter) was conducted with Hematoxylin and Eosin (H&E) staining. Masson's trichrome (Masson) staining was employed to determine renal fibrotic changes, and Periodic Acid-Schiff (PAS) staining was conducted to determine basal membrane thickness. After staining, the preparations were examined with a microscopic image analysis system (ZEISS Axiolab 5, Carl Zeiss Microscopy GmbH, Jena, Germany). Detailed H&E, Masson, and PAS staining protocols are presented in the **Supplementary Material** (Supplemental methods for histopathological examinations).

Determination of TGF-β1 and β-Catenin mRNA Expressions with Quantitative Real-Time Polymerase Chain Reaction (qRT-PCR)

Initially, total RNA was isolated from the kidney tissues. Samples with optical density of 1.8–2.0 were considered pure, and cDNA was amplified in these samples. Then, amplification was conducted with Real-Time PCR and TaqMan primers/probes that target *TGF-β1* and *β-catenin* genes. Relative expression levels of the investigated genes were determined with the $2^{-\Delta\Delta Ct}$ method. The commercial kit instructions and the primer target gene sequences are presented in the **Supplementary Material** (**Supplementary Tables 1**,**2**).

Measurement of Renal Klotho Protein Levels with the ELISA Method

Klotho protein levels were measured with the sandwich enzyme linked immunosorbent assay (ELISA) method in kidney tissues. Tissue homogenization, total protein measurements (bicinchoninic acid (BCA) protein assay), and klotho protein determinations were conducted based on the manufacturer protocols. Klotho protein levels were presented as "ng/mg protein", normalized for the total protein content. Commercial ELISA kit protocols are presented in the **Supplementary Material** (**Supplementary Table 1**).

Determination of the SIRT2 Protein Expression with Western Blotting

Tissues homogenized in RIPA Lysis Buffer that included protease and phosphatase inhibitors were quantified for total protein with the BCA Protein Assay. Protein (20 µg) was separated from equal samples with sodium dodecyl sulfate-polyacrylamide gel electrophoresis (SDS-PAGE, 12%) and transferred onto nitrocellulose membranes. Membranes were blocked in Tris-Buffered Saline with Tween 20 (TBST) that included 5% non-fat milk powder at +4 °C overnight. After blocking, membranes were sequentially incubated with primary antibodies (Anti-SIRT2, 1:500, sc-28298, Santa Cruz Biotechnology, Dallas, TX, USA, anti-beta-actin, 1:500, sc-47778, Santa Cruz Biotechnology, Dallas, TX, USA) and horseradish peroxidase (HRP)-conjugated secondary antibody (Anti-mouse, 1:2000, Cat. # 62-6520, Invitrogen, Thermo Fisher Scientific Inc., Cambridge, MA, USA) for 1.5 hours. The protein bands were visualized with a Chemiluminescent kit on the membranes. The bands were analyzed with the iBrightTM imaging system (# FL 1500, Thermo Fisher Scientific Inc.,

Journal of
BIOLOGICAL REGULATORS
and Homeostatic Agents

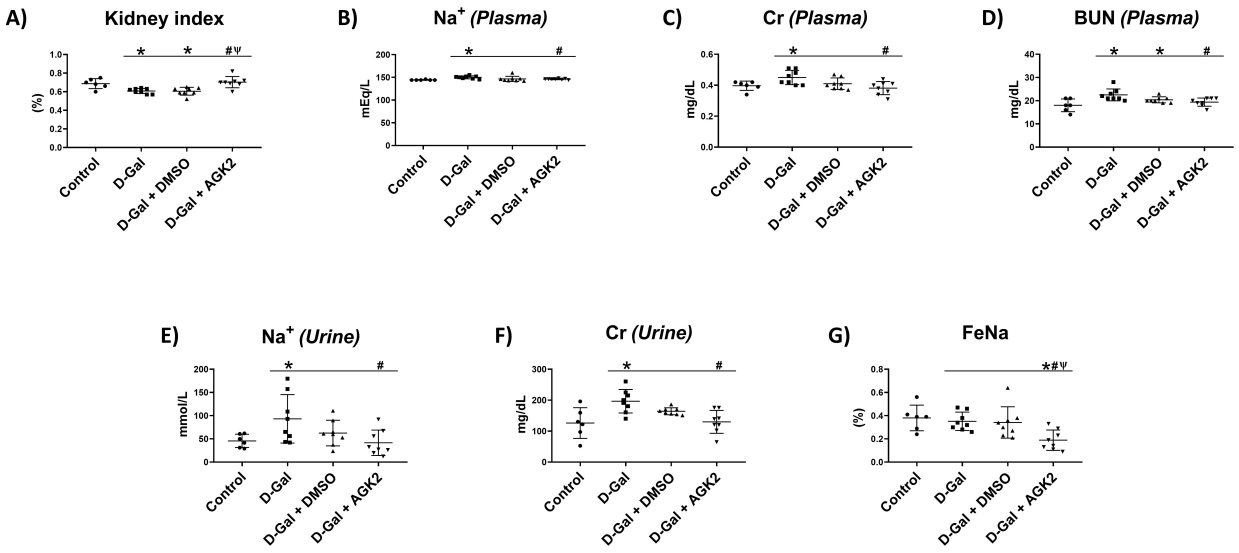

Fig. 1. Kidney index and renal function markers. The changes in the kidney index (A), plasma sodium (Na^+) (B), plasma creatinine (Cr) (C), blood urea nitrogen (BUN) (D), urinary Na^+(E), urinary creatinine (F), and fractional excretion of sodium (FeNa%) (G) in saline treatment (control, n = 6), D-galactose (D-Gal, n = 8), D-galactose and 4% DMSO-PBS (D-Gal+DMSO, n = 8), and D-galactose and AGK-2 (D-Gal+AGK2, n = 8) groups. *, #, and Ψ denote significant differences at $p < 0.05$ level when compared to the control, D-Gal, and D-Gal+DMSO groups, respectively. PBS, phosphate-buffered saline; DMSO, dimethyl sulfoxide; AGK, acylglycerol kinase.

Cambridge, MA, USA). Details of the employed antibodies and kits are presented in the **Supplementary Material** (**Supplementary Table 1**).

Immunohistochemical Analysis

Kidney sections were prepared for immunohistochemical analysis after deparaffinization and dehydration. Antigens were retrieved with high-temperature citrate buffer (pH 6.0) treatment. The tissues were then passed through distilled water, and the peripheral tissues were delineated with a PAP pen. The tissues were washed with PBS, and incubated for 10 minutes in 3% hydrogen peroxide to block endogenous peroxidase activity. Then, they were rewashed with PBS. The immunohistochemical analysis continued with the Ultra Vision Detection System Large Volume Anti-Polyvalent, HRP kit, and the sections were incubated overnight at +4 °C with primary antibodies (β-catenin, klotho, SIRT2, fibronectin) at an adequate dilution (1:100). The slides were washed with PBS, and a biotinylated secondary antibody was applied for 10 minutes, and the slides were rewashed with PBS. The tissues were then exposed to the streptavidin-peroxidase enzyme complex for 10 minutes, followed by a final wash with PBS. Visible immunoreaction was induced with the DAB substrate chromogen. Mayer's Hematoxylin was employed as the counterstain. After they were kept in xylene and sealed with entellan, the slides were examined with the ZEISS Axiolab 5 computer-assisted light microscope and analyzed with Zen Blue 3.4 software (Carl Zeiss Microscopy GmbH, Jena, Germany). After the immunohistochemical analysis of the primary antibodies, the immune-positive density was determined with Image J software [26]. Details of the employed antibodies are presented in **Supplementary Material** (**Supplementary Table 1**).

TUNEL Assay

The terminal deoxynucleotidyl transferase deoxyuridine triphosphate (dUTP) nick end labeling (TUNEL) method was employed to detect DNA fragmentation, and induced apoptosis in tissue samples. After deparaffinization, sections were passed through a series of alcohols, washed with PBS, and then the tissue perimeters were marked with a PAP pen. Then, the process continued with the ApopTag Peroxidase In Situ Apoptosis Detection kit (Cat: S7101, Millipore, Temecula, CA, USA). After they were incubated in xylene and sealed with Entellan, the slides were viewed with the ZEISS Axiolab 5 computer-assisted light microscope and analyzed with Zen Blue 3.4 software (Carl Zeiss Microscopy GmbH, Jena, Germany). TUNEL-positive cells were analyzed in five randomly selected areas at 400× magnification [27].

Statistical Analysis

The study data were analyzed with the SPSS 22 software (IBM SPSS statistics, Chicago, IL, USA). All data are presented as group "means ± standard deviations". One-way ANOVA (post hoc LSD) was employed for inter-group comparisons. Pearson's correlation coefficient (r) was calculated to determine the correlations between the variables. $p < 0.05$ was considered statistically significant.

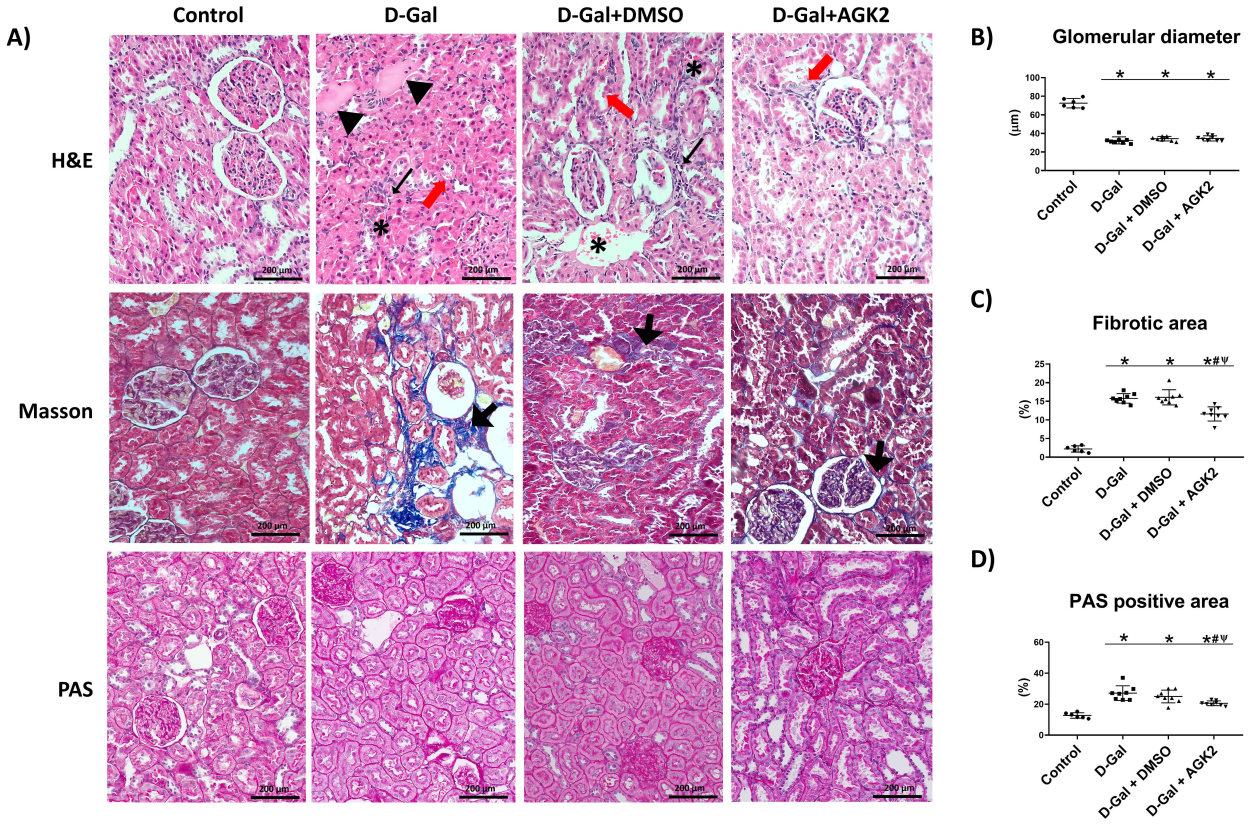

Fig. 2. Histopathological changes. Hematoxylin and Eosin (H&E), Masson's Trichrome (Masson), or Periodic Acid-Schiff (PAS) staining micrographs (Scale bar: 200 µm) (A). The changes in the glomerular diameter (B), fibrotic area (C), and PAS-positive area (D) were analyzed with H&E, Masson, and PAS staining in the saline (control, n = 6), D-galactose (D-Gal, n = 8), D-galactose and 4% DMSO-PBS (D-Gal+DMSO, n = 8), and D-galactose and AGK-2 (D-Gal+AGK2, n = 8) groups, respectively. Inflammatory cell infiltration (thin arrow), congestion (*), vacuolar degeneration (red arrow), tubular thyroidization (▼), fibrotic area (thick arrow). *, $^{\#}$ and $^{\Psi}$ denote significant differences ($p < 0.05$) when compared to the control, D-Gal, and D-Gal+DMSO groups, respectively.

Results

Changes in Kidney Index and Renal Function Markers

The kidney index was significantly lower in the D-Gal and D-Gal+DMSO groups when compared to the control group ($p = 0.004$, $p = 0.003$, respectively). However, the kidney index was significantly higher in the D-Gal+AGK2 group when compared to the D-Gal and D-Gal+DMSO groups ($p < 0.001$, $p < 0.001$, respectively) (Fig. 1A).

Plasma Na^+ and Cr levels were higher in the D-Gal group when compared to the control group ($p = 0.006$, $p = 0.021$, respectively) and lower in the D-Gal+AGK2 group when compared to the D-Gal group ($p = 0.031$, $p = 0.002$, respectively) (Fig. 1B,C).

BUN levels were higher in the D-Gal and D-Gal+DMSO groups when compared to the control group ($p = 0.001$, $p = 0.049$, respectively) but lower in the D-Gal+AGK2 group when compared to the D-Gal group ($p = 0.007$) (Fig. 1D).

Urine Na and Cr levels were higher in the D-Gal group when compared to the control group ($p = 0.017$, $p = 0.001$, respectively) and lower in the D-Gal+AGK2 group when compared to the D-Gal group ($p = 0.006$, $p = 0.001$, respectively) (Fig. 1E,F).

FeNa% was lower in the D-Gal+AGK2 group when compared to all other groups (control, D-Gal, and D-Gal+DMSO) ($p = 0.002$, $p = 0.005$, $p = 0.007$, respectively) (Fig. 1G).

Histopathological Changes

As seen in Fig. 2, the kidney presented a normal histologic appearance in the control group. Congestion, degeneration of the tubules, thyroidization of the tubules, and inflammatory cell infiltration were observed in the D-Gal and D-Gal+DMSO groups. However, these pathological changes ameliorated with AGK-2 administration. In the H&E staining analysis of the kidney tissue sections, it was observed that the glomerular diameter was significantly lower in the D-Gal, D-Gal+DMSO, and D-Gal+AGK2 groups when compared to the control group ($p < 0.001$, $p < 0.001$, $p < 0.001$, respectively) (Fig. 2A,B).

Masson staining revealed that the fibrotic area (%) was significantly greater in the D-Gal, D-Gal+DMSO, and D-

Journal of
BIOLOGICAL REGULATORS
and Homeostatic Agents

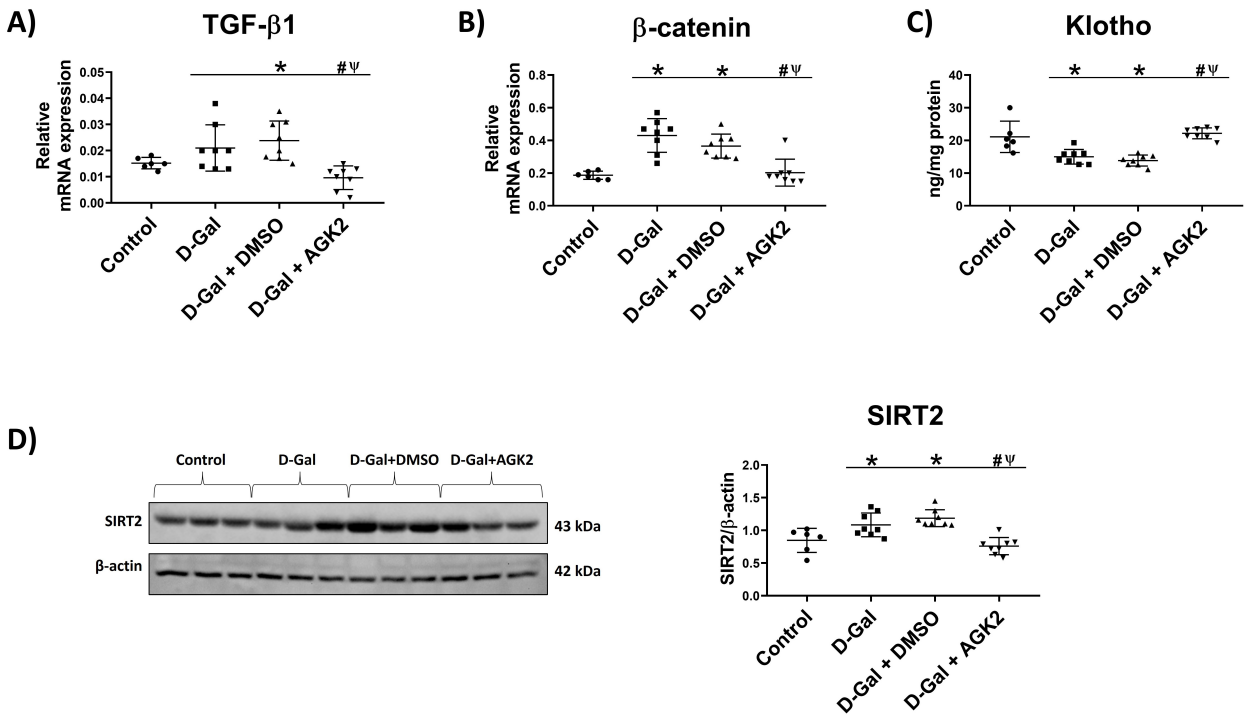

Fig. 3. The changes in TGF-β1, β-catenin, klotho, and SIRT2. The changes in relative TGF-β1 (A) and β-catenin (B) mRNA expressions, klotho protein levels (C), and SIRT2 protein expressions (D) in saline (control, n = 6), D-galactose (D-Gal, n = 8), D-galactose and 4% DMSO-PBS (D-Gal+DMSO, n = 8), and D-galactose and AGK-2 (D-Gal+AGK2, n = 8) groups. *, $^{\#}$ and $^{\Psi}$ denote significant differences ($p < 0.05$) when compared to the control, D-Gal, and D-Gal+DMSO groups. TGF-β1, transforming growth factor-β1. SIRT2, silent mating type information regulation 2 homolog-2.

Gal+AGK2 groups when compared to the control group ($p < 0.001$, $p < 0.001$, $p < 0.001$, respectively). In the D-Gal+AGK2 group, the fibrotic area (%) was smaller when compared to the D-Gal and D-Gal+DMSO groups ($p < 0.001$, $p < 0.001$, respectively) (Fig. 2A,C).

The calculation of the PAS-positive area (%) to determine the basal membrane thickness revealed that the PAS-positive area (%) was significantly greater in the D-Gal, D-Gal+DMSO, and D-Gal+AGK2 groups when compared to the control group ($p < 0.001$, $p < 0.001$, $p < 0.001$, respectively). In the D-Gal+AGK2 group, the PAS-positive area (%) was smaller when compared to the D-Gal and D-Gal+DMSO groups ($p = 0.001$, $p = 0.017$, respectively) (Fig. 2A,D).

Changes in Renal TGF-β1 and β-Catenin mRNA Expressions, Klotho Protein Levels, and SIRT2 Protein Expressions

TGF-β1 mRNA expression was significantly higher in the kidney tissues of the D-Gal+DMSO group when compared to the control ($p = 0.022$). It was significantly lower in the D-Gal+AGK2 group when compared to the D-Gal and D-Gal+DMSO groups ($p = 0.002$, $p < 0.001$, respectively) (Fig. 3A).

β-catenin mRNA expression was higher in the D-Gal and D-Gal+DMSO groups when compared to the control group ($p < 0.001$, $p < 0.001$, respectively). It was significantly lower in the D-Gal+AGK2 group when compared to both the D-Gal and D-Gal+DMSO groups ($p < 0.001$, $p < 0.001$, respectively) (Fig. 3B).

Klotho protein levels were lower in the D-Gal and D-Gal+DMSO groups when compared to the control group ($p < 0.001$, $p < 0.001$, respectively). Klotho levels were significantly higher in the D-Gal+AGK2 group when compared to the D-Gal and D-Gal+DMSO groups ($p < 0.001$, $p < 0.001$, respectively) (Fig. 3C).

SIRT2 protein expression was higher in the D-Gal and D-Gal+DMSO groups when compared to the control group ($p = 0.009$, $p < 0.001$, respectively). SIRT2 expression was significantly lower in the D-Gal+AGK2 group when compared to the D-Gal and D-Gal+DMSO groups ($p < 0.001$, $p < 0.001$, respectively) (Fig. 3D).

There were positive correlations between SIRT2, TGF-β1, and β-catenin and a negative correlation between SIRT2 and klotho ($r = 0.521$ $p = 0.003$, $r = 0.55$ $p = 0.002$, $r = -0.634$ $p < 0.001$, respectively). There was a positive correlation between TGF-β1 and β-catenin and a negative correlation between TGF-β1 and klotho ($r = 0.475$ $p = 0.008$, $r = -0.579$ $p = 0.001$, respectively) (Fig. 4).

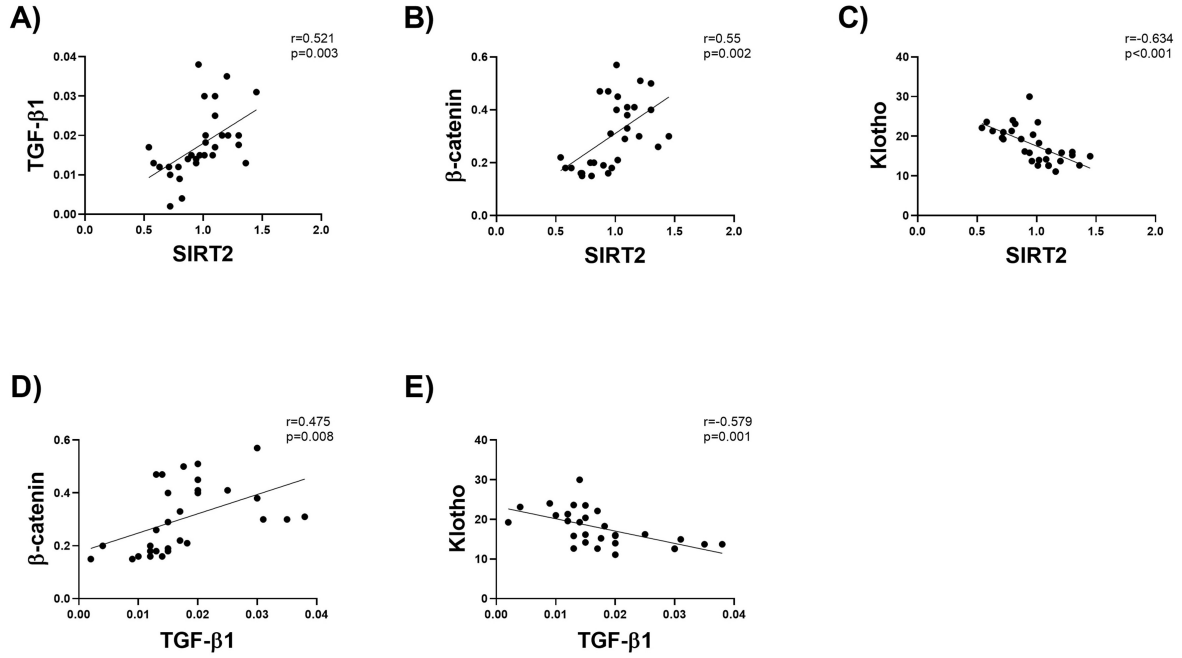

Fig. 4. Correlations between study variables. There were positive correlations between SIRT2 and TGF-β1 (A) and β-catenin (B) and there was a negative correlation between SIRT2 and klotho (C). There was a positive correlation between TGF-β1 and β-catenin (D) and a negative correlation between TGF-β1 and klotho (E).

Immunoreactivity of β-Catenin, Klotho, SIRT2, and Fibronectin, and Apoptotic Changes in Kidney

The immune-positive β-catenin region (%) was significantly greater in the D-Gal, D-Gal+DMSO, and D-Gal+AGK2 groups when compared to the control group ($p < 0.001$, $p < 0.001$, $p = 0.027$, respectively). It was significantly smaller in the D-Gal+AGK2 group when compared to the D-Gal and D-Gal+DMSO groups ($p = 0.006$, $p = 0.006$, respectively) (Fig. 5A,B).

The immune-positive klotho region (%) was significantly smaller in the D-Gal, D-Gal+DMSO, and D-Gal+AGK2 groups when compared to the control group ($p = 0.008$, $p = 0.009$, $p = 0.04$, respectively) (Fig. 5A,C).

The immune-positive SIRT2 region (%) was significantly greater in the D-Gal group when compared to the control group ($p = 0.009$). It was significantly smaller in the D-Gal+AGK2 group when compared to all other groups (control, D-Gal, and D-Gal+DMSO) ($p < 0.001$, $p < 0.001$, $p < 0.001$, respectively) (Fig. 5A,D).

The immune-positive fibronectin region (%) was significantly greater in the D-Gal, D-Gal+DMSO, and D-Gal+AGK2 groups when compared to the control group ($p < 0.001$, $p < 0.001$, $p < 0.001$, respectively). It was significantly smaller in the D-Gal+AGK2 group when compared to the D-Gal and D-Gal+DMSO groups ($p < 0.001$, $p = 0.002$, respectively) (Fig. 5A,E).

TUNEL-positive cell count was significantly higher in the D-Gal, D-Gal+DMSO, and D-Gal+AGK2 groups when compared to the control ($p < 0.001$, $p < 0.001$, $p < 0.001$, respectively) (Fig. 6).

Discussion

D-galactose administration (with or without 4% DMSO) reduced kidney index when compared to the control rats. It increased urinary Na^+ and Cr levels, renal function indicators, and plasma Na^+, Cr, and BUN levels. Histopathological analysis revealed that D-galactose reduced glomerular diameter and increased basal membrane thickness and fibrotic area. D-galactose administration increased SIRT2 protein expression and immunoreactivity, TGF-β1 mRNA expression, β-catenin mRNA expression and immunoreactivity, and fibronectin immunoreactivity and decreased klotho protein level and immunoreactivity when compared to the control. Furthermore, D-galactose administration increased the TUNEL-positive cell count, indicating an increase in apoptosis.

D-Gal and AGK-2 co-administration led to a higher kidney index when compared to D-galactose administration (with or without 4% DMSO). Urinary Na^+ and Cr levels and plasma Na^+, Cr, and BUN levels were lower in the D-Gal and AGK-2 group when compared to the D-galactose group. There were no significant differences between the control and D-galactose group FeNa% findings; however, AGK-2 and D-galactose co-administration reduced FeNa% when compared to the control and D-galactose groups. AGK-2 did not significantly improve the D-galactose-induced decrease in glomerular diameter; however, it reduced basal membrane thickness and fibrotic area. AGK-2 also decreased the D-galactose-induced increase in SIRT2, TGF-β1, β-catenin, and fibronectin, while

Journal of
BIOLOGICAL REGULATORS
and Homeostatic Agents

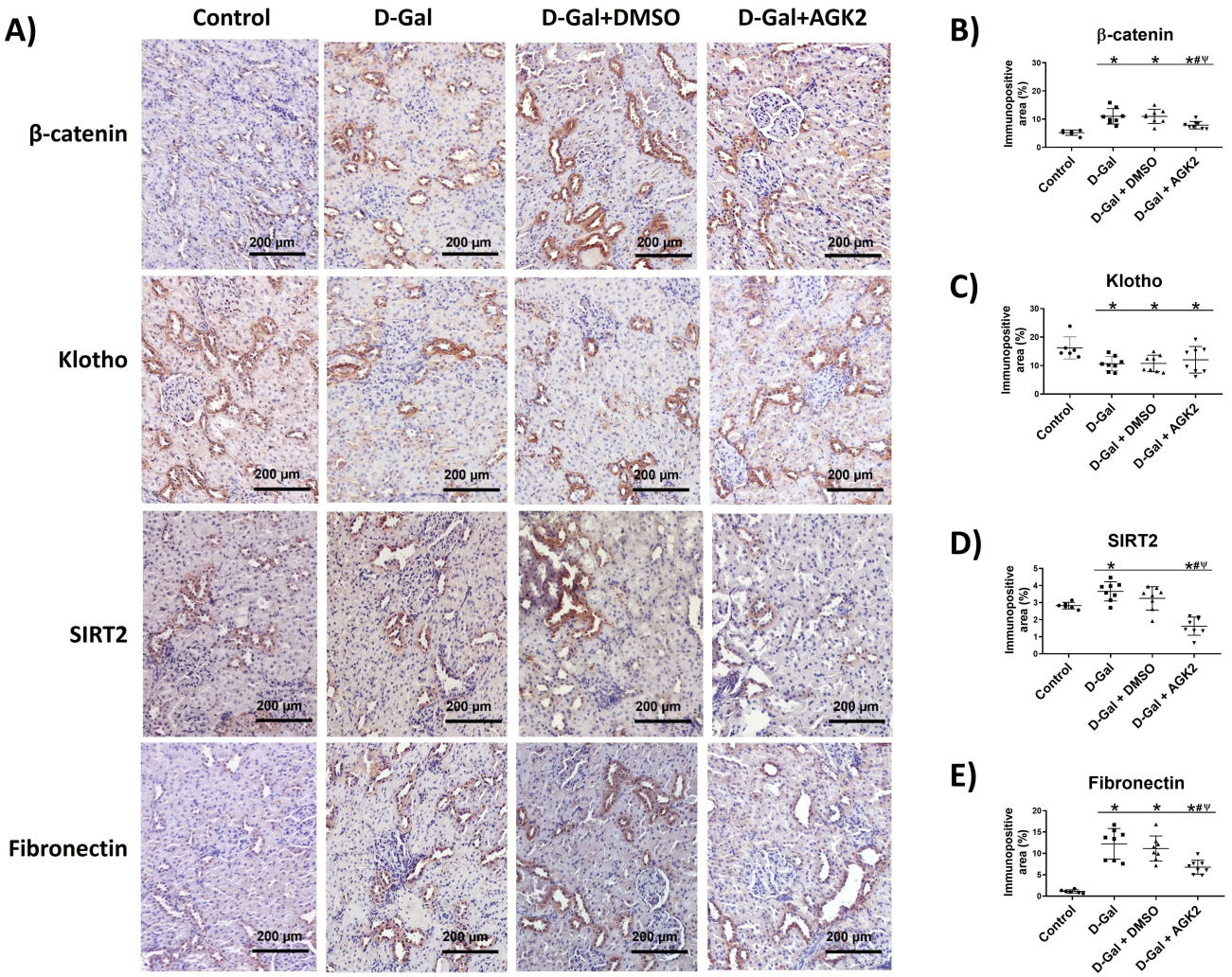

Fig. 5. Immunoreactivity of β-catenin, klotho, SIRT2, and fibronectin. Immunohistochemical staining micrographs for β-catenin, klotho, SIRT2, and fibronectin (Scale bar: 200 μm) (A). The changes in the immune-positive β-catenin (B), klotho (C), SIRT2 (D), and fibronectin (E) regions in saline (control, n = 6), D-galactose (D-Gal, n = 8), D-galactose and 4% DMSO-PBS (D-Gal+DMSO, n = 8), and D-galactose and AGK-2 (D-Gal+AGK2, n = 8) groups. *, $^{\#}$ and $^{\Psi}$ denote significant differences ($p < 0.05$) when compared to the control, D-Gal, and D-Gal+DMSO groups.

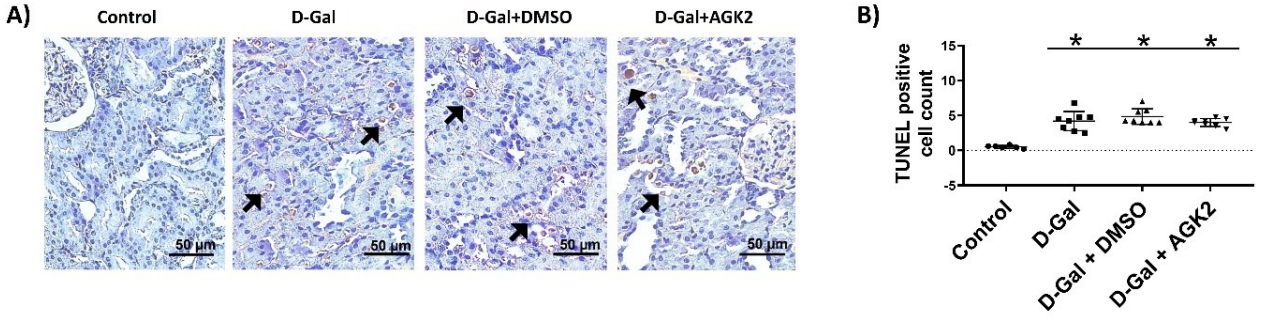

Fig. 6. Apoptosis in the kidney. Photomicrographs of TUNEL-stained kidney tissue sections (→) (Scale bar: 50 μm) (A) and changes in the TUNEL positive cell count (B) in the saline (control, n = 6), D-galactose (D-Gal, n = 8), D-galactose and 4% DMSO-PBS (D-Gal+DMSO, n = 8), and D-galactose and AGK-2 (D-Gal+AGK2, n = 8) groups. * denote significant differences ($p < 0.05$) when compared to the control group. TUNEL, terminal deoxynucleotidyl transferase deoxyuridine triphosphate (dUTP) nick end labeling.

increasing the low klotho levels. AGK-2 relatively reduced the TUNEL-positive cell count, which increased by about five times in the D-galactose groups, although the reduction was not statistically significant.

A low kidney index, indicating a reduction in the kidney coefficient, is one of the most significant indicators of aging [10]. Previous studies reported a D-galactose-induced decrease in kidney index in aging models, in addition to natural aging [3]. The current study demonstrated that the kidney index decreased with D-galactose administration, while AGK-2 alleviated the decrease.

Elevated sugar levels and kidney injuries disrupt sodium homeostasis [28]. It was demonstrated that D-galactose administration increased kidney damage markers such as urea, BUN creatinine, uric acid, and Cys-C in mice [4,6]. The current study findings demonstrated that plasma and urine Na, Cr, and BUN levels increased with D-galactose administration, and AGK-2 alleviated these findings. Urinary biochemical analyses are primarily used to differentiate transient (reversible, prerenal) and persistent (established, postrenal) kidney damage. FeNa is among the primary biochemical urinary markers used for this purpose. Although FeNa% measurements were not reported in D-galactose-treated rat models, early studies demonstrated that FeNa was lower than 1% in prerenal azotemia patients and higher than 3% in acute tubular necrosis patients [29]. It was demonstrated that a lower than 1% FeNa indicates prerenal azotemia and acute glomerulonephritis, while a FeNa greater than 1% indicates acute tubular necrosis and urinary system obstruction [30]. Although there is currently no consensus on FeNa%, it is generally accepted that a FeNa less than 1% indicates transient acute kidney injury [5]. In the present study, the mean FeNa was below 1% across all groups, and AGK-2 and D-galactose co-administration reduced fractional sodium excretion when compared to all other groups, including the control group.

Functional renal mass, renal blood flow, and GFR decrease with age. This is often accompanied by glomerular basal membrane thickening, glomerulosclerosis, tubular atrophy, interstitial fibrosis, and increased apoptosis [6,31]. The D-galactose-induced aging model leads to histological changes in the kidney such as decreases in glomerular count and diameter, increases in sclerotic glomeruli count and diameter, and expansion of the renal capsule [4]. Furthermore, aging is associated with a reduction in renal antioxidant capacity [4], autophagy [32], and the anti-aging protein klotho signal [33], while fibrosis was associated with an increase in angiotensin-II sensitivity, inflammation, pericyte activation, ROS, apoptosis, TGF-β, and Wnt/β-catenin signaling pathways [31,34].

TGF-β1 is considered the "master regulator" in the development of glomerular and tubulointerstitial fibrosis [8]. An increase in TGF-β signaling was noted to contribute to cellular degeneration, tissue fibrosis, inflammation, reduced regenerative capacity, and metabolic dysfunction [35]. TGF-β1, secreted by renal tubular and interstitial cells, leads to the development of tubulointerstitial fibrosis through fibroblast activation, accompanied by an elevation in SIRT2 levels [19]. In the obstructive nephropathy model, it was demonstrated that SIRT2 inhibition reduced the differentiation of the fibroblasts into myoblasts and the formation of collagen and fibronectin [22].

The decline in the expression of klotho with age, an anti-aging protein that prevents cellular aging, apoptosis, and fibrogenesis, was associated with the deterioration of kidney functions with age [13,15]. A correlation was demonstrated between reduced kidney functions and low serum-soluble klotho levels in elderly individuals [33]. High renal apoptosis and fibrosis and a decrease in klotho levels were reported in a D-galactose-induced aging model in mice [6]. In fact, Klotho is a Wnt/β-catenin signaling pathway antagonist [14].

The present study demonstrated that D-galactose administration reduced kidney index, induced histopathological changes, promoted fibrosis, and increased renal fibronectin and apoptosis. Furthermore, D-galactose administration led to a decrease in klotho levels and improved TGF-β1/β-catenin signaling. A negative correlation was also observed between TGF-β1/β-catenin signaling and klotho. We could not identify a study in the literature demonstrating the antifibrotic protective effect of SIRT2 inhibition in the D-galactose-induced renal aging model. However, our findings indicated that SIRT2 inhibition effectively improved the deterioration induced by D-galactose. The co-administration of D-galactose and AGK-2, a specific SIRT2 inhibitor, inhibited renal SIRT2 protein expression and immunoreactivity. It was also observed that D-galactose administration increased renal SIRT2, suggesting that SIRT2 mediated the regulation of TGF-β1/β-catenin and klotho signaling during the development of histopathological changes, primarily fibrosis, and age-related decline in renal functions.

SIRT2 is expressed in metabolically active organs such as the kidney, liver, pancreas, testes, and adipose tissue [16,18]. In mice, it was reported that SIRT2 increased with cranial and spinal aging in cranial regions such as the cerebral cortex and hippocampus [24,36]. No previous studies reported an increase in renal SIRT2 expression after D-galactose administration; however, it was demonstrated that SIRT2 mRNA expression was significantly higher in the brain tissues of 24 months old naturally aged rats and D-Gal administered 4 months old rats when compared to 4 months old rats [37].

Among the seven members of the sirtuin family, it was demonstrated that SIRT2 was the most sensitive sirtuin to hypertensive renal damage in mice, and its expression increased [38]. In SIRT2 knockout and transgenic mice, it was demonstrated that the SIRT2/mitogen-activated protein kinase phosphatase-1 (MKP-1) pathway mediated cisplatin-induced acute kidney injury [39], and

Journal of
BIOLOGICAL REGULATORS
and Homeostatic Agents

the inhibition of the SIRT2/MDM2 signal was protective against renal fibrosis [40]. On the other hand, a study reported that SIRT2 was downregulated in cisplatin-induced acute kidney injury [41]. In hyperglycemic MPC-5 murine kidney foot cells, it was reported that SIRT2 was upregulated as autophagy decreased and apoptosis increased [42]. Also, it was reported that SIRT2 inactivation was protective against renal ischemia/reperfusion injury [43]. Furthermore, due to the predominance of elderly donors in kidney transplants, it was suggested that the expressions of a certain group of genes (*CDKN2A*, *CDKN1A*, *POT1*), including SIRT2, in pre-transplant kidney biopsies that indicate cellular damage and biological aging, could predict post-transplant organ functions [44].

He *et al*. [19] demonstrated that SIRT2 expression in the renal tubulointerstitium was higher in tubulointerstitial fibrosis patients and in mice with unilateral urethral obstruction (UUO). Furthermore, they demonstrated that genetic or AGK-2-induced pharmacological inhibition of SIRT2 inhibited TGF-β1-induced fibroblast activation [19]. On the other hand, in cultured tubular epithelial cells (NRK-52E) exposed to TGF-β1, there was an increase in α-SMA, collagen III, and fibronectin levels. However, AGK-2 and TGF-β1 co-administration did not significantly improve these figures. Nevertheless, AGK-2 and TGF-β1 co-administration effectively reduced α-SMA, collagen III, and fibronectin levels in renal interstitial fibroblasts (NRK-49F) [19]. Ponnusamy *et al*. [22] demonstrated that AGK-2 inhibited renal fibroblast activation based on dose and time, reducing α-SMA, collagen I, and fibronectin expressions.

Our previous studies demonstrated that SIRT2 inhibition had antioxidant and antiapoptotic effects on the naturally aging brain [24,25]. Furthermore, we demonstrated its antifibrotic effectiveness in rat liver tissues in a D-Galactose-induced aging model, as well as its ability to increase klotho levels [21]. In mice, AGK-2-mediated SIRT2 inhibition reduced pulmonary fibrosis by decreasing TGF-β1-induced phosphorylation of Smad2/3 [20,23]. These findings suggested that SIRT2 inhibition via the modulation of fibrotic signaling pathways could exhibit antifibrotic effects on the kidney, liver, and lungs.

Conclusion

The present study findings indicated SIRT2 involvement in age-induced renal fibrosis and demonstrated that SIRT2 inhibition could improve renal dysfunction, histopathological findings, fibrosis, and alterations in related signaling pathways associated with aging. Thus, we could suggest that SIRT2 inhibition may represent a novel clinical therapeutic strategy for age-related kidney diseases. However, further studies should be conducted with the activators and inhibitors of relevant signaling pathways should be conducted to elucidate the role of SIRT2 in age-related decline in renal functions. The limitations of the current study primarily stemmed from the inability to demonstrate the direct impact of the TGF-β1, Wnt/β-catenin, and klotho signal activators and/or inhibitors, and the analysis of apoptosis solely with the TUNEL method.

Availability of Data and Materials

All data included in this study are available upon request by contact with the corresponding author.

Author Contributions

AKA and KGA contributed to the concept and designed the research study. AKA, ANB, FGS and SÖAD performed the research. AKA and KGA contributed to the analysis and interpretation of the data. AKA wrote the first draft of the manuscript, and all authors commented on previous versions. All authors contributed to editorial changes in the manuscript. All authors read and approved the final manuscript. All authors have participated sufficiently in the work to take public responsibility for appropriate portions of the content and agreed to be accountable for all aspects of the work in ensuring that questions related to its accuracy or integrity.

Ethics Approval and Consent to Participate

The rats were kept based on the European Convention ETS 123 guidelines and all study methods were approved by the Gazi University Animal Experiments Ethics Committee (G.U.ET-20.011).

Acknowledgment

Not applicable.

Funding

This study was supported by Gazi University Scientific Research Projects Commission under grant number 5953.

Conflict of Interest

All authors have completed the ICMJE uniform disclosure form. The authors have no conflicts of interest to declare.

Supplementary Material

Supplementary material associated with this article can be found, in the online version, at https://doi.org/10.23812/j.biol.regul.homeost.agents.20233711.580.

References

[1] Centers for Disease Control and Prevention (CDC). Chronic kidney disease in the United States. 2023. Available at: https://www.cdc.gov/kidneydisease/publications-resources/CKD-national-facts.html (Accessed: 20 August 2023).

[2] World Health Organization (WHO). The top 10 causes of death. 2020. Available at: https://www.who.int/news-room/fact-sheets/detail/the-top-10-causes-of-death (Accessed: 20 August 2023).

[3] Mo ZZ, Liu YH, Li CL, Xu LQ, Wen LL, Xian YF, *et al*. Protective Effect of SFE-CO_2 of Ligusticum chuanxiong Hort Against d-Galactose-Induced Injury in the Mouse Liver and Kidney. Rejuvenation Research. 2017; 20: 231–243.

[4] Fan Y, Xia J, Jia D, Zhang M, Zhang Y, Huang G, *et al*. Mechanism of ginsenoside Rg1 renal protection in a mouse model of d-galactose-induced subacute damage. Pharmaceutical Biology. 2016; 54: 1815–1821.

[5] Lima C, Macedo E. Urinary Biochemistry in the Diagnosis of Acute Kidney Injury. Disease Markers. 2018; 2018: 4907024.

[6] Lan KC, Peng PJ, Chang TY, Liu SH. Resveratrol Alleviates Advanced Glycation End-Products-Related Renal Dysfunction in D-Galactose-Induced Aging Mice. Metabolites. 2023; 13: 655.

[7] Sun C, Tian X, Jia Y, Yang M, Li Y, Fernig DG. Functions of exogenous FGF signals in regulation of fibroblast to myofibroblast differentiation and extracellular matrix protein expression. Open Biology. 2022; 12: 210356.

[8] Meng XM, Nikolic-Paterson DJ, Lan HY. TGF-β: the master regulator of fibrosis. Nature Reviews. Nephrology. 2016; 12: 325–338.

[9] Gewin L. The many talents of transforming growth factor-β in the kidney. Current Opinion in Nephrology and Hypertension. 2019; 28: 203–210.

[10] Azman KF, Zakaria R. D-Galactose-induced accelerated aging model: an overview. Biogerontology. 2019; 20: 763–782.

[11] Liu B, Tu Y, He W, Liu Y, Wu W, Fang Q, *et al*. Hyperoside attenuates renal aging and injury induced by D-galactose via inhibiting AMPK-ULK1 signaling-mediated autophagy. Aging. 2018; 10: 4197–4212.

[12] Miao J, Liu J, Niu J, Zhang Y, Shen W, Luo C, *et al*. Wnt/β-catenin/RAS signaling mediates age-related renal fibrosis and is associated with mitochondrial dysfunction. Aging Cell. 2019; 18: e13004.

[13] Semba RD, Cappola AR, Sun K, Bandinelli S, Dalal M, Crasto C, *et al*. Plasma klotho and mortality risk in older community-dwelling adults. The Journals of Gerontology. Series A, Biological Sciences and Medical Sciences. 2011; 66: 794–800.

[14] Zhou L, Li Y, Zhou D, Tan RJ, Liu Y. Loss of Klotho contributes to kidney injury by derepression of Wnt/β-catenin signaling. Journal of the American Society of Nephrology: JASN. 2013; 24: 771–785.

[15] Doi S, Zou Y, Togao O, Pastor JV, John GB, Wang L, *et al*. Klotho inhibits transforming growth factor-beta1 (TGF-beta1) signaling and suppresses renal fibrosis and cancer metastasis in mice. The Journal of Biological Chemistry. 2011; 286: 8655–8665.

[16] Gupta R, Ambasta RK, Kumar P. Multifaced role of protein deacetylase sirtuins in neurodegenerative disease. Neuroscience and Biobehavioral Reviews. 2022; 132: 976–997.

[17] Zullo A, Mancini FP, Schleip R, Wearing S, Klingler W. Fibrosis: Sirtuins at the checkpoints of myofibroblast differentiation and profibrotic activity. Wound Repair and Regeneration: Official Publication of the Wound Healing Society [and] the European Tissue Repair Society. 2021; 29: 650–666.

[18] Wu QJ, Zhang TN, Chen HH, Yu XF, Lv JL, Liu YY, *et al*. The sirtuin family in health and disease. Signal Transduction and Targeted Therapy. 2022; 7: 402.

[19] He FF, You RY, Ye C, Lei CT, Tang H, Su H, *et al*. Inhibition of SIRT2 Alleviates Fibroblast Activation and Renal Tubulointerstitial Fibrosis via MDM2. Cellular Physiology and Biochemistry: International Journal of Experimental Cellular Physiology, Biochemistry, and Pharmacology. 2018; 46: 451–460.

[20] Gong H, Zheng C, Lyu X, Dong L, Tan S, Zhang X. Inhibition of Sirt2 Alleviates Fibroblasts Activation and Pulmonary Fibrosis *via* Smad2/3 Pathway. Frontiers in Pharmacology. 2021; 12: 756131.

[21] Bahar AN, Keskin-Aktan A, Sonugur FG, Akarca Dizakar SÖ, Akbulut KG. Effect of sirt2 inhibition on developing fibrosis in d-galactose induced aging. Acta Physiologica. 2023: 237; 22.

[22] Ponnusamy M, Zhou X, Yan Y, Tang J, Tolbert E, Zhao TC, *et al*. Blocking sirtuin 1 and 2 inhibits renal interstitial fibroblast activation and attenuates renal interstitial fibrosis in obstructive nephropathy. The Journal of Pharmacology and Experimental Therapeutics. 2014; 350: 243–256.

[23] Kim YY, Hur G, Lee SW, Lee SJ, Lee S, Kim SH, *et al*. AGK2 ameliorates mast cell-mediated allergic airway inflammation and fibrosis by inhibiting FcεRI/TGF-β signaling pathway. Pharmacological Research. 2020; 159: 105027.

[24] Keskin-Aktan A, Akbulut KG, Abdi S, Akbulut H. SIRT2 and FOXO3a expressions in the cerebral cortex and hippocampus of young and aged male rats: antioxidant and anti-apoptotic effects of melatonin. Biologia Futura. 2022; 73: 71–85.

[25] Akbulut KG, Keskin-Aktan A, Abgarmi SA, Akbulut H. The role of SIRT2 inhibition on the aging process of brain in male rats. Aging Brain. 2023; 4: 100087.

[26] Guiteras R, Sola A, Flaquer M, Hotter G, Torras J, Grinyó JM, *et al*. Macrophage Overexpressing NGAL Ameliorated Kidney Fibrosis in the UUO Mice Model. Cellular Physiology and Biochemistry: International Journal of Experimental Cellular Physiology, Biochemistry, and Pharmacology. 2017; 42: 1945–1960.

[27] Xiao C, Zhao H, Zhu H, Zhang Y, Su Q, Zhao F, *et al*. Tisp40 Induces Tubular Epithelial Cell GSDMD-Mediated Pyroptosis in Renal Ischemia-Reperfusion Injury via NF-κB Signaling. Frontiers in Physiology. 2020; 11: 906.

[28] Dominguez Rieg JA, Rieg T. What does sodium-glucose cotransporter 1 inhibition add: Prospects for dual inhibition. Diabetes, Obesity & Metabolism. 2019; 21 Suppl 2: 43–52.

[29] Espinel CH. The FENa test. Use in the differential diagnosis of acute renal failure. JAMA. 1976; 236: 579–581.

[30] Espinel CH, Gregory AW. Differential diagnosis of acute renal failure. Clinical Nephrology. 1980; 13: 73–77.

[31] Portilla D. Apoptosis, fibrosis and senescence. Nephron. Clinical Practice. 2014; 127: 65–69.

[32] Lenoir O, Tharaux PL, Huber TB. Autophagy in kidney disease and aging: lessons from rodent models. Kidney International. 2016; 90: 950–964.

[33] Drew DA, Katz R, Kritchevsky S, Ix J, Shlipak M, Gutiérrez OM, *et al*. Association between Soluble Klotho and Change in Kidney Function: The Health Aging and Body Composition Study. Journal of the American Society of Nephrology: JASN. 2017; 28: 1859–1866.

[34] Xu J, Zhou L, Liu Y. Cellular Senescence in Kidney Fibrosis: Pathologic Significance and Therapeutic Strategies. Frontiers in Pharmacology. 2020; 11: 601325.

[35] Tominaga K, Suzuki HI. TGF-β Signaling in Cellular Senescence and Aging-Related Pathology. International Journal of Molecular Sciences. 2019; 20: 5002.

[36] Keskin-Aktan A, Akbulut KG, Yazici-Mutlu Ç, Sonugur G, Ocal M, Akbulut H. The effects of melatonin and curcumin on the expression of SIRT2, Bcl-2 and Bax in the hippocampus of adult rats. Brain Research Bulletin. 2018; 137: 306–310.

[37] Singh S, Singh AK, Garg G, Rizvi SI. Fisetin as a caloric restric-

Journal of
BIOLOGICAL REGULATORS
and Homeostatic Agents

tion mimetic protects rat brain against aging induced oxidative stress, apoptosis and neurodegeneration. Life Sciences. 2018; 193: 171–179.

[38] Zhang Y, Zhang N, Zou Y, Song C, Cao K, Wu B, *et al*. Deacetylation of Septin4 by SIRT2 (Silent Mating Type Information Regulation 2 Homolog-2) Mitigates Damaging of Hypertensive Nephropathy. Circulation Research. 2023; 132: 601–624.

[39] Jung YJ, Park W, Kang KP, Kim W. SIRT2 is involved in cisplatin-induced acute kidney injury through regulation of mitogen-activated protein kinase phosphatase-1. Nephrology, Dialysis, Transplantation: Official Publication of the European Dialysis and Transplant Association - European Renal Association. 2020; 35: 1145–1156.

[40] Ahmedy OA, El-Tanbouly DM, Al-Mokaddem AK, El-Said YAM. Insights into the role of P2X7R/DUSP6/ERK1/2 and SIRT2/MDM2 signaling in the nephroprotective effect of berberine against cisplatin-induced renal fibrosis in rats. Life Sciences. 2022; 309: 121040.

[41] Peng L, Liu D, Liu H, Xia M, Wan L, Li M, *et al*. Bombesin receptor-activated protein exacerbates cisplatin-induced AKI by regulating the degradation of SIRT2. Nephrology, Dialysis, Transplantation: Official Publication of the European Dialysis and Transplant Association - European Renal Association. 2022; 37: 2366–2385.

[42] Liu S, Gao X, Fan Z, Wang Q. SIRT2 Affects Cell Proliferation and Apoptosis by Suppressing the Level of Autophagy in Renal Podocytes. Disease Markers. 2022; 2022: 4586198.

[43] Wang Y, Wu CJ, Du Y, Liu YQ, Cai JR, Wu XQ, *et al*. SIRT2 tyrosine nitration by peroxynitrite in response to renal ischemia/reperfusion injury. Free Radical Research. 2021; 55: 1104–1118.

[44] McGlynn LM, Stevenson K, Lamb K, Zino S, Brown M, Prina A, *et al*. Cellular senescence in pretransplant renal biopsies predicts postoperative organ function. Aging Cell. 2009; 8: 45–51.